J. Biochem. 123, 62-70 (1998)

Solution Structure of CINC/Gro Investigated by Heteronuclear NMR

Hiroyuki Hanzawa,* Hideyuki Haruyama,*,[1] Kiyoshi Konishi,† Kazuyoshi Watanabe,‡ and Susumu Tsurufuji‡

*Analytical and Metabolic Research Laboratories, Sankyo Co., Ltd., 2-58, Hiromachi 1-chome, Shinagawa-ku, Tokyo 140; †Department of Biochemistry, Toyama Medical and Pharmaceutical University Faculty of Medicine, Sugitani, Toyama 930-01; and ‡Institute of Cytosignal Research, Inc., Hiromachi, Shinagawa-ku, Tokyo 140

Received for publication, June 30, 1997

Cytokine-induced neutrophil chemoattractant (CINC/Gro) is a chemotactic factor for neutrophils in the rat and a member of the CXC chemokine family. The refined three-dimensional structure of CINC/Gro was derived with the aid of heteronuclear magnetic resonance spectroscopy and a hybrid method of distance geometry and simulated annealing. The backbone atomic r.m.s. differences for 19 structures about the mean coordinates for residues 7 to 70 are 0.69±0.15 Å for the dimer and 0.56±0.13 Å for the monomer. The N terminal region containing an ELR sequence, an essential motif for chemotactic activity, is disordered in solution, as in other CXC chemokines. The dimer structure consists of a six-stranded anti-parallel β sheet with two C-terminal α helices on the β sheet. The overall dimer structure of CINC/Gro is similar to that of human MGSA, though the backbone r.m.s.d.s between CINC/Gro and the two MGSA structures were high (1.81 and 2.34 Å for the monomer) in spite of the high sequence homology (67%). The major difference resides in the relative position of the C-terminal α helix with respect to the β sheet. This results in a difference of interhelical distances in the dimer: wider (15 Å) in CINC/Gro, as in IL-8, than in MGSA (11.7 and 10 Å).

Key words: chemokine, dimer, inflammation, NMR.

CINC/Gro, alternatively referred to as CINC-1, is a chemotactic factor for neutrophils that is produced in rat renal epithelial cells and cells of the normal rat kidney epithelial cell line NRK-52E in response to lipopolysaccharides, tumor necrosis factor-α and interleukin 1β (*1*). CINC/Gro is now recognized as the rat counterpart of human MGSA/Gro, based on its high degree of sequence homology (*2*). A rat counterpart of interleukin 8 has not been found so far, while CINC homologues, CINC-2α, CINC-2β, and CINC-3, have been identified (*3*).

The margination of neutrophils in postcapillary venules and their migration through the vascular endothelium is a key phenomenon in acute inflammation, in which chemotactic factors for neutrophils play a major role. Among CXC chemokines, IL-8 has been extensively studied (*4*).

The three-dimensional structure of human IL-8 has been determined by NMR spectroscopy (*5*) and X-ray crystallography (*6*). The direct structural analysis of the complex formed with IL-8 and its receptor, however, is unrealistic, because chemokine receptors identified as IL-8RA and IL-8RB are G-protein coupled seven transmembrane proteins, the structural determination of which is a demanding task with currently available technology.

IL-8RA is a highly selective receptor for IL-8 and has two-hundred-fold reduced affinity for MGSA, the structure of which has also been determined by NMR by Fairbrother *et al.* (1mgs.pdb) (*7*) and Kim *et al.* (1MSG.pdb) (*8*), while IL-8RB has equivalent affinity for both IL-8 and MGSA (*9, 10*). Alternatively, an analysis using chimera receptors consisting of the IL-8RA portion and the IL-8RB portion in various combinations indicated that the N-terminal extracellular domain of the receptors may be responsible for their different selectivities to IL-8 and MGSA (*11, 12*).

Furthermore, a titration study of ^{15}N-labeled IL-8 with the peptide corresponding to the N-terminal extracellular domain of IL-8RA revealed that ^{15}N and NH chemical shift changes were not observed in the ELR sequence, an essential motif for biological activity (*13, 14*), but in the long loop region preceding the first β strand, indicating the presence of a second binding region on IL-8 (*15*).

In an attempt to expand our understanding of the mechanism of chemokine/chemokine receptor interaction at the atomic level, comparative studies between the CINC/Gro-CINC receptor system and the IL-8-IL-8 receptor system have been undertaken. ^1H-NMR resonance assignments and the preliminary three-dimensional structure of CINC/Gro, which exhibits essentially the same overall folding as other CXC chemokines, including IL-8 and MGSA, were reported previously (*16*). However, knowledge of the overall folding is not sufficient for an understanding of the interaction of CXC chemokines and their receptors. For IL-8 and MGSA, small differences in their second binding region were shown to be responsible for the receptor binding specificity (*17*).

In this report, the three-dimensional structure of CINC/

[1] To whom correspondence should be addressed.

Abbreviations: MGSA, melanoma growth-stimulating activity; HOHAHA, homonuclear Hartman-Hahn spectroscopy; NMR, nuclear magnetic resonance; NOESY, nuclear Overhauser enhancement spectroscopy; PF-4, platelet factor 4.

Gro has been refined using heteronuclear multi-dimensional NMR techniques and a structural comparison of IL-8 and MGSA is presented.

MATERIALS AND METHODS

Expression and purification of recombinant CINC/Gro from *Escherichia coli* were carried out as described elsewhere with the following modifications (*18*): after having been harvested, cells were ultrasonicated and centrifuged at 10,000 rpm, and the supernatant was applied to a CM Sepharose column equilibrated with 50 mM Tris-HCl at pH 7.5. CINC/Gro was eluted with the same buffer containing 500 mM NaCl in a stepwise manner. After dialysis and freeze-drying, HPLC analysis was performed. Uniform $^{15}N/^{13}C$ labeling was carried out by growing the cells in minimal medium with $^{15}NH_4Cl$ and ^{13}C-glucose as the sole nitrogen and carbon sources, respectively. About 2 mg protein was obtained per 1 liter culture. A fractional ^{13}C-labeled CINC/Gro was obtained using minimal medium in which the sole carbon source was 10% ^{13}C-glucose and 90% isotopically normal glucose.

Samples were lyophilized and dissolved in 100% D_2O or 90% H_2O-10% D_2O and the pH was adjusted to 5.3. The concentration of the protein was 2 mM for heteronuclear experiments and 5 mM for homonuclear experiments.

NMR measurements were carried out using JEOL GSX-500 and A500 spectrometers. Homonuclear 2D and 3D NMR experiments were performed as described previously (*16*). E.COSY spectra were acquired with 256×2,048 complex data points and zero-filled to 1,028×8,192 data points for measurement of coupling constants (*19*). ^1H-^{15}N HSQC and HMQC-J spectra were obtained with a spectral width of 2,500 Hz in F_1(N) and 7,000 Hz in F_2(H) (*20, 21*).

3D constant-time HNCO, HNCA, and HN(CO)CA spectra were acquired using a triple resonance $^1H/^{15}N/^{13}C$ probe (*22*). The ^1H,^{15}N carriers were placed at the water frequency and 118 ppm, respectively. The ^{13}C carrier was placed at 180 ppm for HNCO and 50 ppm for HNCA and HN(CO)CA. The acquired data matrix was 32 (t_1)×64 (t_2)×512 (t_3) complex data points with spectral widths of 2,500, 2,500, and 7,000 Hz in the F_1(^{15}N), F_2(^{13}C), and F_3(^1H) dimensions, respectively.

3D HCCH-TOCSY spectra were recorded using a DIPSI-3 sequence in which ^{13}C pulses were applied with a 10 kHz RF field for isotropic mixing using a TH probe (*23*). Mixing times of HCCH-TOCSY were 10 and 20 ms. The ^1H carrier was placed at 2.9 ppm and the ^{13}C carrier was placed at 42 ppm. The acquired data matrix was 96 (t_1)×32 (t_2)×512 (t_3) complex data points and was zero-filled to 128×64×512 data points. Spectral widths were 7,000, 2,500, and 7,000 Hz in the F_1(^1H), F_2(^{13}C), and F_3(^1H) dimensions, respectively.

Interproton distance restraints were derived from NOEs assigned in the 2D NOESY (*24*), 3D HOHAHA-NOESY (*16*), and 3D HMQC-NOESY (*25*) spectra.

2D $^{12}C/^{13}C$ doubly half filtered NOESY spectra were recorded (*26*) using 1 : 1 mixtures of ^{13}C-labeled and non-labeled CINC/Gro.

Hydrogen bonds were assigned from the hydrogen/deuterium exchange experiments and NOE connectivities. An amide proton which was observed in HOHAHA spectra recorded 2 h after the sample was dissolved in D_2O at 313 K, was considered a possible hydrogen bond donor.

One- and two-dimensional spectra were processed using NMR1 and NMR2 software on a DEC station 5000/200 computer, respectively, while all 3D spectra were processed using Felix software. 2D spectra were apotized with a shifted sine bell function and zero-filled to 2 K×2 K points in both dimensions.

The three-dimensional structure of CINC/Gro was determined using the programs DIANA (*27*) and XPLOR (*28*) as described previously (*16*). The monomer structures were constructed from random conformations by DIANA, then dimer structures were constructed using intersubunit NOEs by coordinate duplication, rotation and translation. From these dimer structures, dynamical simulated annealing calculations were performed according to the protocol of Clore *et al.* (*5*). For maintaining symmetry between the subunits, non-crystallographic symmetry was used throughout the simulated annealing calculation with a force constant of 300 kcal/mol.

The pK_a values of His19 and His34 were obtained from the chemical shifts of C2 protons in the pH titration experiments in D_2O. The pK_as (H_2O) were calibrated as pK_a (H_2O) = pK_a (D_2O) − 0.2 (*29*). The distance of closest approach for the two α-helix axes was calculated using the method of Chothia *et al.* (*30*).

RESULTS AND DISCUSSION

Spectral Assignments and Structural Refinement—Based on the ^1H assignments previously reported (*16*), the sequential assignments of the backbone (and the side chain) amide nitrogens other than Pro were directly obtained from the ^1H-^{15}N HSQC spectrum. Sequential assignment of backbone ^{13}C resonances was performed using the HNCO, HNCA, HN(CO)CA spectra. An example of the ^1H-^{13}C slices at 127 ppm (^{15}N) in the HNCA spectrum is shown in Fig. 1. Ten intraresidual cross signals were observed on this

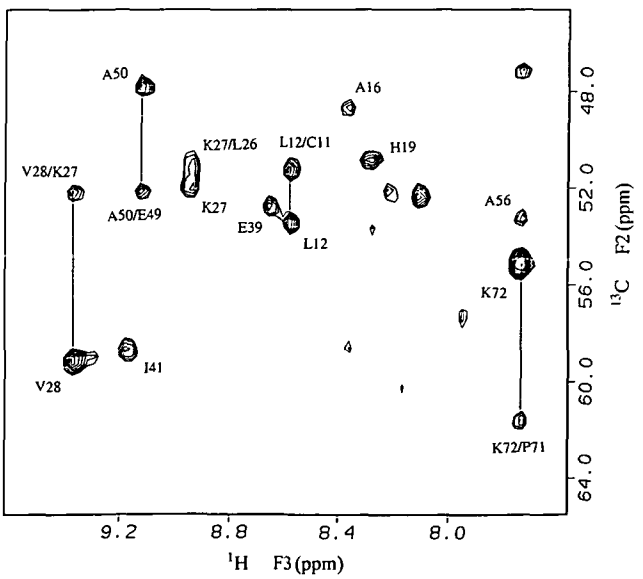

Fig. 1. **An example of the F2-F3 slicing of the HNCA spectrum at 127 ppm (^{15}N).** Those cross signals with one residue name are intraresidual and those with two sequential residue names are interresidual signals.

slice and, for V28, A50, K27, L12, and K72, interresidual signals were also observed and sequential connectivity from L26 to V28 was identified only from this slice. Side chain ^{13}C, ^{1}H assignments were made using HCCH-COSY and HCCH-TOCSY spectra.

The stereospecific assignments of 14 β methylene proton pairs out of 28 non-equivalent β methylenes were made based upon $^{3}J_{\alpha\beta}$ coupling constants and intraresidual and sequential NOEs observed in the NOESY spectrum with a mixing time of 70 ms. Most of the $^{3}J_{\alpha\beta}$ coupling constants were derived from the E.COSY spectrum, while some of those with broad line widths were semi-quantitatively evaluated by comparing the intensities of cross peaks between the amide and β protons in the 3D-TOCSY-HMQC spectrum (*31*). Stereospecific assignment of methyl resonances of Leu was performed according to the method described by Senn *et al.* using fractionally ^{13}C-labeled CINC/Gro (*32*).

The NOEs were classified according to their intensities as strong, medium, weak, and very weak. Upper limits of the distance constraints for weak and very weak NOEs were 5 and 6 Å, respectively. For intra and sequential NOEs, 2.7 and 3.5 Å were used as the upper limits of strong and medium NOEs, while the upper bounds of strong and medium NOEs were 3 and 4 Å for other NOEs (*i.e.* $|i-j|>1$), respectively.

Intersubunit NOEs which had been indirectly assigned by elimination were directly confirmed by double-half filter experiments using 1 : 1 mixtures of ^{13}C-labeled and non-labeled CINC/Gro (*26*). Figure 2a shows an example of an F1:^{12}C filtered/F2:^{13}C filtered NOESY spectrum. Among the αH-αH NOEs characteristic of the anti-paralel β sheet structure which appeared in the corresponding region of the NOESY (Fig. 2b), the NOE between αH of Ser25 and αH of Met29 was identified as inter-subunit NOE. At the final round of refinement, weak NOEs which could not be explained as intrasubunit NOEs were assigned as intersubunit NOEs.

A set of 720 interproton constraints per monomer and 29 intersubunit NOEs were obtained. Intrasubunit distance constraints involve 190 intraresidue NOEs and 203 sequential ($|i-j|=1$), 132 short-range ($|i-j|\leq 5$), and 195 long-range ($|i-j|>5$) interresidue NOEs. Information on 20 hydrogen bonds and 63 dihedral angle constraints per monomer was also used.

Monomer structures were constructed using DIANA (*27*) with the REDAC option (*33*). After several rounds of calculations, 50 monomer structures with the smallest target functions were accepted. The initial dimer structures constructed as described previously were refined by simulated annealing calculations. Nineteen structures

TABLE I. **Structural statistics of 19 converged structures.**

R.m.s. deviation from experimental distance restraints (Å)		
NOE (720)	0.0265±0.007	
R.m.s. deviation from experimental dihedral restraints (°)		
ϕ, χ^1 (63)	0.407±0.044	
Deviations from idealized covalent geometry		
Bonds (Å)	0.009±0.001	
Angles (°)	2.77±0.03	
Impropers (°)	0.31±0.02	
Energies (kcal·mol^{-1})		
F_{NOE}	55.6±2.84	
F_{CDIH}	0.013±0.003	
F_{NCS}	0.17±0.04	
F_{repel}	35.0±1.6	
F_{bond}	32.6±2.2	
F_{ang}	454.9±9.8	
F_{imp}	8.2±1.0	
Atomic r.m.s. differences (Å) to mean structure		
	Backbone (N, Cα, C)	All heavy atoms
Dimer	0.69±0.15	1.09±0.11
Monomer	0.56±0.11	1.00±0.10

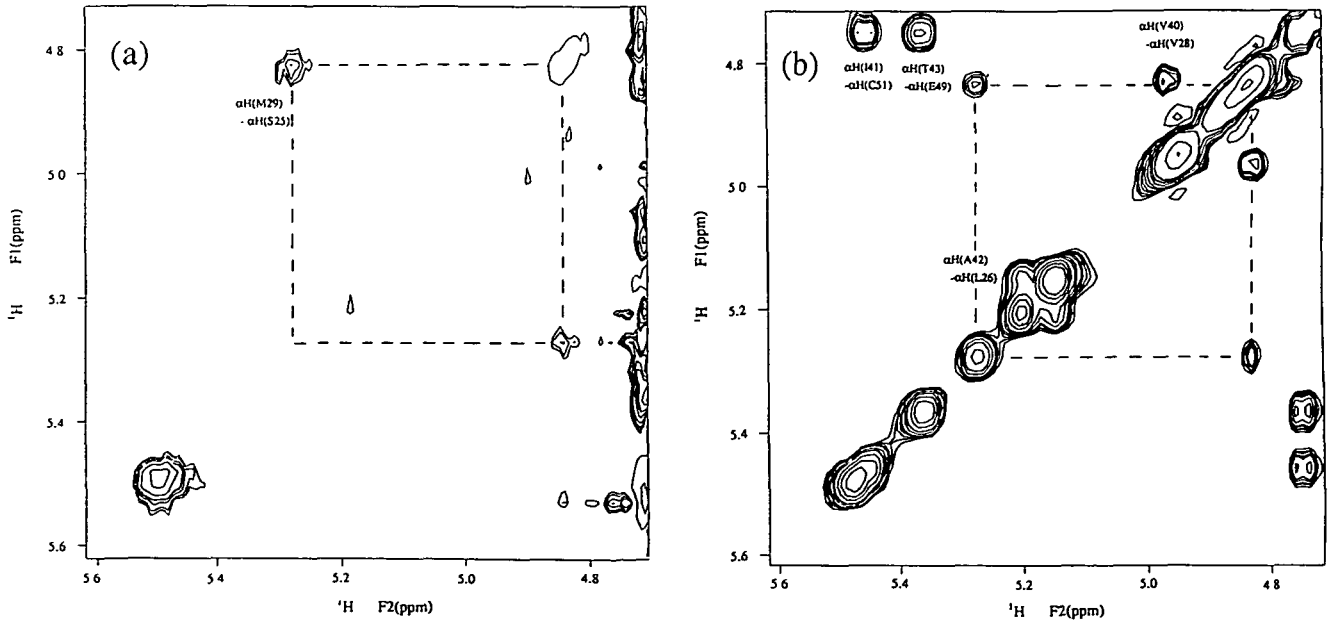

Fig. 2. **(a) αH-αH region of 2D $^{12}C/^{13}C$ doubly filtered NOESY spectrum of CINC/Gro.** Protein concentration was 1 mM. **(b) The same region of the ^{1}H-^{1}H NOESY spectrum.** Inter- and intra-subunit NOEs were differentiated by comparison of the two spectra. In both spectra, the mixing time of 150 ms was employed.

satisfying the experimental constraints were accepted. The structural statistics of the 19 structures of CINC/Gro are summarized in Table I. There were no interproton distance constraints violated by more than 0.5 Å, nor torsional angle constraints by more than 5°.

Atomic r.m.s. differences for the 19 dimer structures about the mean coordinates were 0.69±0.15 Å for the backbone atoms and 1.09±0.11 Å for all heavy atoms between Leu7 and Val70. For monomers, r.m.s. differences are 0.56±0.11 Å for the backbone and 1.00±0.10 Å for all heavy atoms.

The atomic r.m.s. deviations for backbone and heavy atoms and angular order parameters for ϕ, φ, and $\chi 1$ torsion angles are plotted in Fig. 3. The angular order parameter S is a statistical parameter defining the precision of the torsion angle, where $S=1$ indicates a uniformly defined angle and $S=0$ a completely randomized angle (*34*). Order parameters for both ϕ and φ were more than 0.9 in all but three regions, including the N-terminal, the C-terminal, and the loop between 30 and 38, which had a well-defined backbone structure.

Effect of Refinement by Heteronuclear Experiment—Isotope labeling and heteronuclear experiments increased the total constraints from 696 to 823 per monomer. Those newly added constraints are 58 intraresidual NOEs, 49 interresidual NOEs, and 14 angle constraints. Intersubunit NOEs were increased from 22 to 29. Due to those increased constraints, r.m.s. differences of the accepted structures between Leu7 and Val70 were decreased from 0.94 to 0.69 Å for backbone atoms and from 1.33 to 1.09 Å for all non hydrogen atoms. Figure 4a shows the three-residual r.m.s. differences of non hydrogen atoms before and after refinement, and Fig. 4b also shows the distribution of constraints per residue, in which newly added ones are indicated as open columns. The resolution of the structural segments of 12-14, 21-23, 33-36, 57-59 was improved; in each of them, about 10 constraints were newly added. The ELR motif and N-terminal long loop region have been assumed to be responsible for the receptor binding. Although the number of constraints was increased due to stereospecific assignment of Leu7 and His34, the ELR motif was not refined further. In the putative second binding region including the N-terminal loop, the number of constraints for the C-terminal α helix was increased. Since this α helix has a contact with the N terminal long loop region, the relative position of the α helix to the loop region was well refined, as shown in Fig. 5, in spite of the fact that the three residual r.m.s.d. were not significantly changed in this region.

Description of the Three-Dimensional Structure of CINC/Gro—The best-fit superposition of backbone atoms on the mean coordinates is shown in Fig. 6. The overall folding of CINC/Gro is similar to those of IL-8, MGSA and PF-4 and the previous structure of CINC/Gro. The three-dimensional structure of CINC/Gro is briefly described below. The monomer consists of a three-stranded antiparallel β sheet and a C-terminal α helix. The β strands are formed from Gln24 to Met29 ($\beta 1$), from Thr38 to Leu44 ($\beta 2$), and from Arg48 to Leu52 ($\beta 3$). In the dimer, the $\beta 1$s face each other to form a six-stranded β sheet on which two α helices from each subunit lie in an anti-parallel fashion.

The NH_2-terminal region is constrained by two disulfide linkages between Cys9 and Cys35, and Cys11 and Cys51. The region preceding Cys9, including the ELR motif, is not well defined, while several weak NOEs from Leu7 and Arg8 to His34, αH and δCH_3 of Leu7 to C2H of His34 and NH of Arg8 to βCH_2 of His34 roughly restrict the spatial relation of the ELR motif to the rest of the well-defined part. Only sequential NOEs were observed for the residues preceding Glu6.

A long loop region from Cys11 to Ile23 (colored blue in Fig. 6) is divided into two segments, one from Cys11 to Ile18 and the other from Ile18 to Ile23, which are separately stabilized by hydrophobic interaction. As shown in Fig. 5, Ile18 and Phe20 form a hydrophobic cluster with Ile62, Lys65, and Met66, the residues belonging to the α helix. Fractional solvent accessibilities of Ile18, Phe20, Ile23, Ile62, and Met66 are below 0.3.

$\beta 1$ and $\beta 2$ are connected by a long loop from Pro30 to Thr38. This loop was not well defined in CINC/Gro. Since the ^1H resonances of Pro residues at 30, 31, and 33 were weak and broad (data not shown), this loop may be flexible in solution.

$\beta 1$ is shorter than the equivalent β strands in MGSA and IL-8, due to the Pro residues at 30 and 31. Since the amide

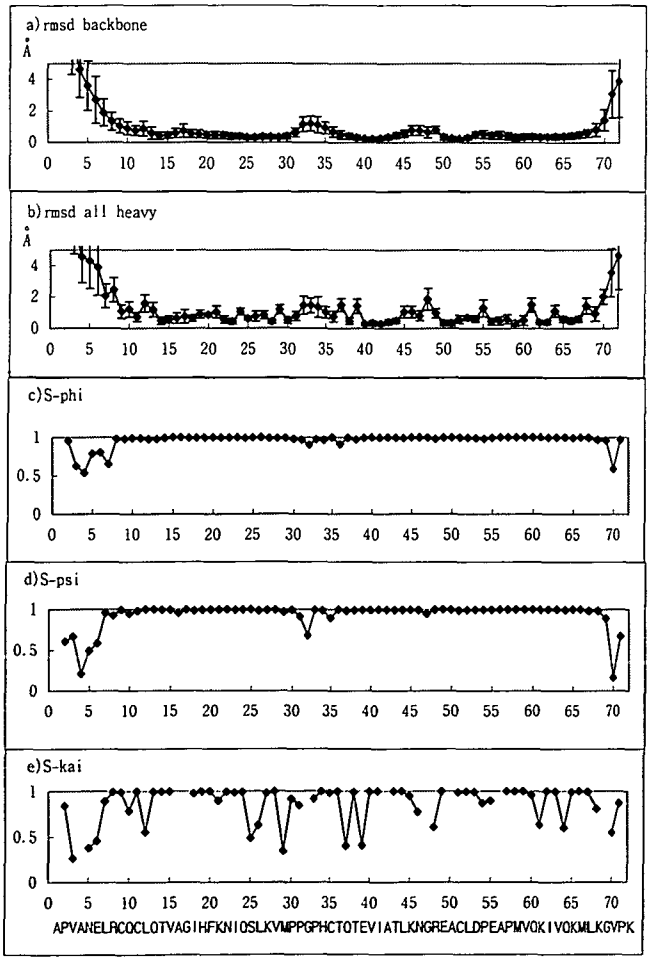

Fig. 3. **Residue-based atomic r.m.s. differences of the 19 individual simulated annealing structures for backbone atoms (a) and for all heavy atoms (b), and angular order parameters for ϕ (c), φ (d), $\chi 1$ (e).** Order parameters of $\chi 1$ for Gly and Ala were set blank. The amino acid sequence of CINC/Gro is also shown in (e).

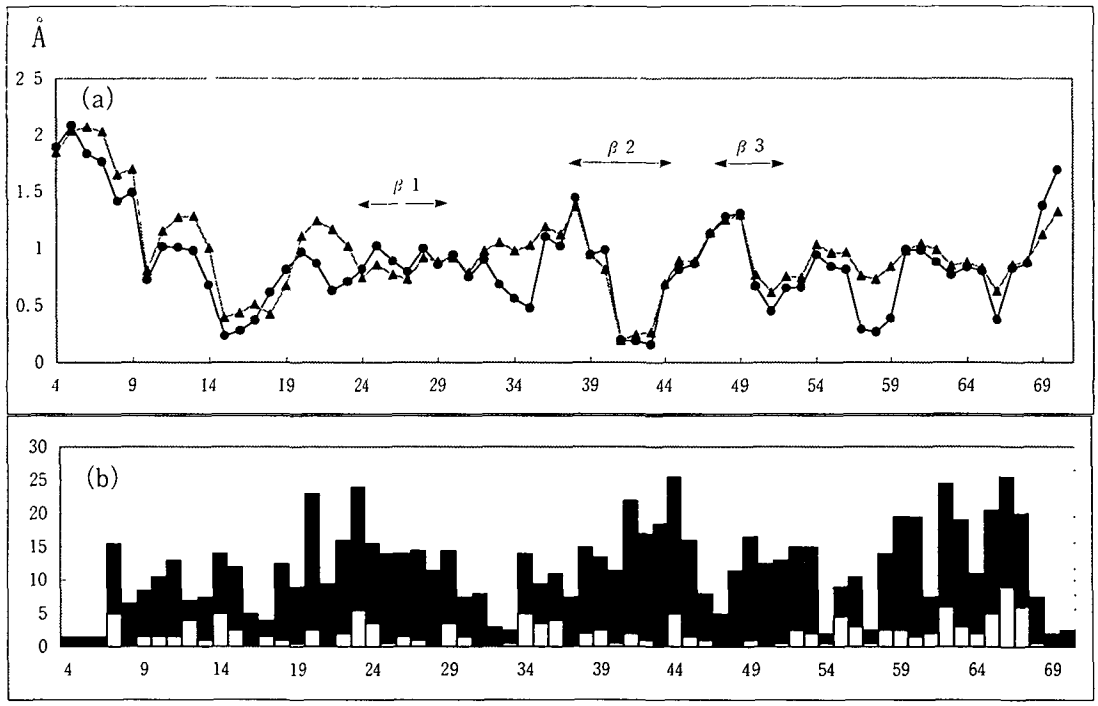

Fig. 4. **(a) The comparison of three residual r.m.s. differences of CINC/Gro before (triangles) and after (circles) refinement by heteronuclear experiments.** Three residual r.m.s. differences were calculated using all heavy atoms after the superpositions were made for the corresponding three residues. **(b) The distribution of the constraints per residue along the sequence.** The open region of the bars corresponds to the newly added constraints in the present calculations.

proton of the corresponding residue in MGSA and IL-8 can participate in the intersubunit hydrogen bonding, the number of intersubunit hydrogen bonds in the β strand interface is reduced from 6 in IL-8 and MGSA, to 4 in CINC/Gro. This is one of the main factors causing the weaker subunit association in CINC/Gro, compared to IL-8 (*35*).

To identify the contact surface involved in the dimer formation, the fractional solvent accessibilities were calculated in both monomer and dimer states of CINC/Gro. If the conformation of the monomeric CINC/Gro does not change significantly in both states as was assumed previously (*35*), Fig. 7 suggests the contact area to involve the residues of strand β1, Thr38, Pro54, and the residues of the C-terminal α helix, especially Met66, Leu67, and Val70. There are ten residues whose solvent accessibility decreases more than 20% on dimer formation. Six of those ten residues are hydrophobic amino acids such as Pro, Leu, and Val. The only charged residue seen in the dimer interface is Lys27, which faces Lys27 of the other monomer causing electrostatic repulsion. Hydrophobic interaction rather than electrostatic interaction contributes to the subunit association as well as the intersubunit hydrogen bonding in the β1 strand (*35*).

Comparison with Other CXC Chemokines—For comparison, the backbone atomic r.m.s. differences between the mean coordinates of CINC/Gro and the structures of IL-8 (*5*), MGSA (*6, 7*), and PF-4 (*36*) were calculated. For MGSA, three-dimensional structures were presented by two groups independently (PDB code: 1mgs.pdb and 1MSG.pdb). The pairwise r.m.s.d.s were calculated for residues 8 to 14 and 19 to 69 according to the method of Fairbrother *et al.* due to a single amino acid insertion in IL-8 (*7*). In spite of the high sequence homology, r.m.s.d. values between MGSA and CINC/Gro were high; 1.81 and 2.34 Å for the monomer and 2.50 and 2.51 Å for the dimer (1mgs.pdb and 1MSG.pdb, respectively). The smallest r.m.s.d. (1.45 Å for the monomer) was calculated between CINC/Gro and PF-4 (sequence homology 39%), which has no chemotactic activities for neutrophils. A value of 1.77 Å for the monomer was obtained between CINC/Gro and IL-8 (sequence homology 47%). Chothia and Lesk elucidated the relationship between sequence identity and r.m.s.d. in homologous proteins, showing that about a 1 Å r.m.s.d. could be attained between proteins with a sequence identity of about 70% (*37*). The observed r.m.s.d. between CINC/Gro and human MGSA was much larger than expected from the sequence identity. The best fit superposition of the monomer of CINC/Gro and MGSAs is shown in Fig. 8.

Figure 9 shows residue-based r.m.s. differences between CINC/Gro and MGSA. Comparisons were performed using two MGSA solution structures solved independently. In the C-terminal α helix, r.m.s.d. values increase towards the C-terminal, showing deviation of the relative position of the α helix with respect to the β sheet. This tendency is discernible for both independently solved MGSA structures. Other major differences between CINC/Gro and MGSA are in the N-terminal loop region and the 30-38 loop. Gly17 shows high r.m.s.d. values for both MGSA structures, and Leu12 and Lys21 show high values between CINC/Gro and 1MSG.pdb. As shown in Fig. 9, these loop regions take different conformations even between the two MGSA structures. An explanation for this could be that the two structures were solved at slightly different pH values

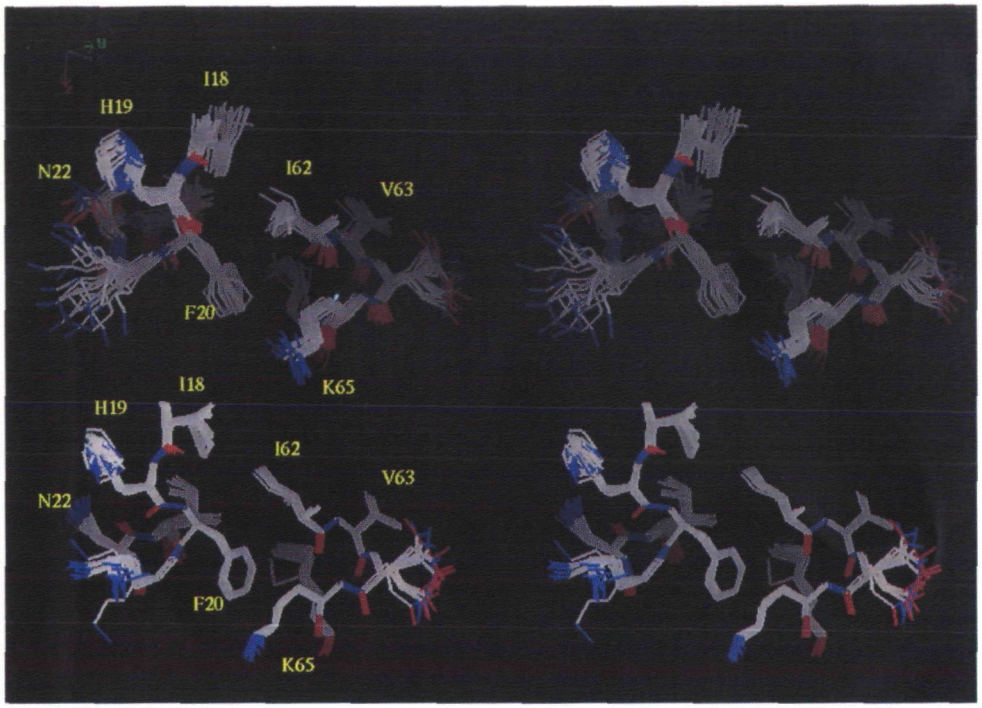

Fig. 5. **Stereoview showing best fit superposition of CINC/Gro before (upper) and after (lower) the refinement using the constraints set given by the present study.** Residual range is from 18 to 23 and from 62 to 66.

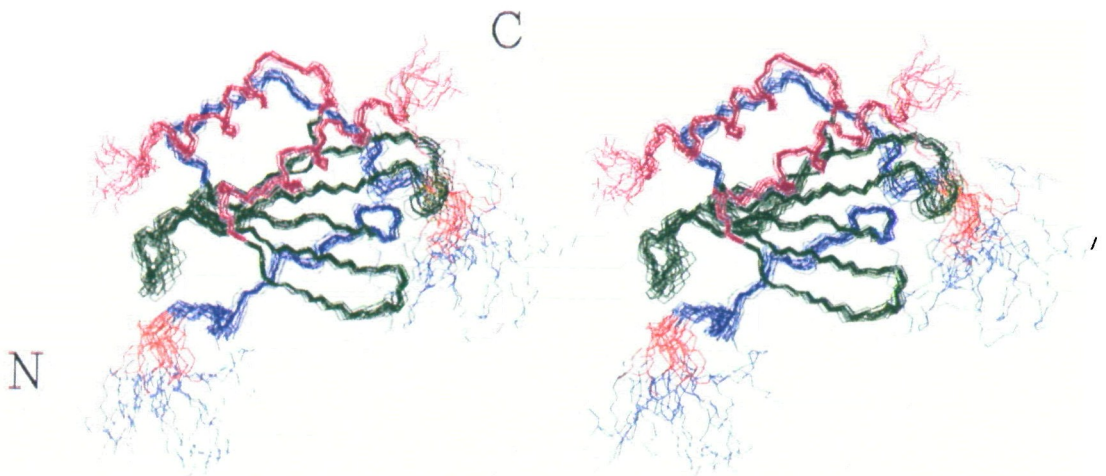

Fig. 6. **Stereoview showing best fit superposition of the backbone atoms of the 19 simulated annealing structures for residues 1 to 72.** The N-terminal region (1 to 23) except for the ELR motif is shown in blue, the ELR motif (6 to 8) in brown, residues 24 to 52 containing β sheets in green and the C-terminal region (52 to 70) containing α helices in purple.

(pH 5.1 and 5.5). The conformation of this loop could be easily affected by solvent conditions. In CINC/Gro, a weak NOE was observed between β methyl protons of Ala16 and the amide proton of Ile18. This NOE could not be explained by the extended conformation observed in MGSA, causing the large r.m.s. difference at Gly17. As shown in Fig. 9, the position of the α helix with respect to the β sheet is shifted along the helix axis.

As noted previously in IL-8, the distance between helices in the structure determined by NMR spectroscopy is wider (15 Å) than that in the structure determined by X ray crystallography (11 Å). The corresponding distances in MGSA are narrow (11.7 and 10 Å) in the structures determined by NMR. On the other hand, the NMR-determined structure of CINC/Gro has a wide interhelical distance (15 Å), like IL-8. In CINC/Gro, interhelical NOE was observed between Leu67 δCH_3 and the ε-amide of Gln60, whereas the corresponding NOE was observed between Leu67 δCH_3 and Lys60 αH in MGSA. Since the distance between Leu67 δCH_3 and Lys60 αH is too far ($\sim$7.5 Å in the current CINC/Gro structure) to give a long-range NOE, the variation of interhelical distances certainly results in the differences of such interhelical NOEs.

On the other hand, the idea that the monomer form binds to its receptor has been accepted on the basis of several lines of evidence, although there is a possibility that IL-8 forms a dimer at the IL-8 receptor site. Ultracentrifugation

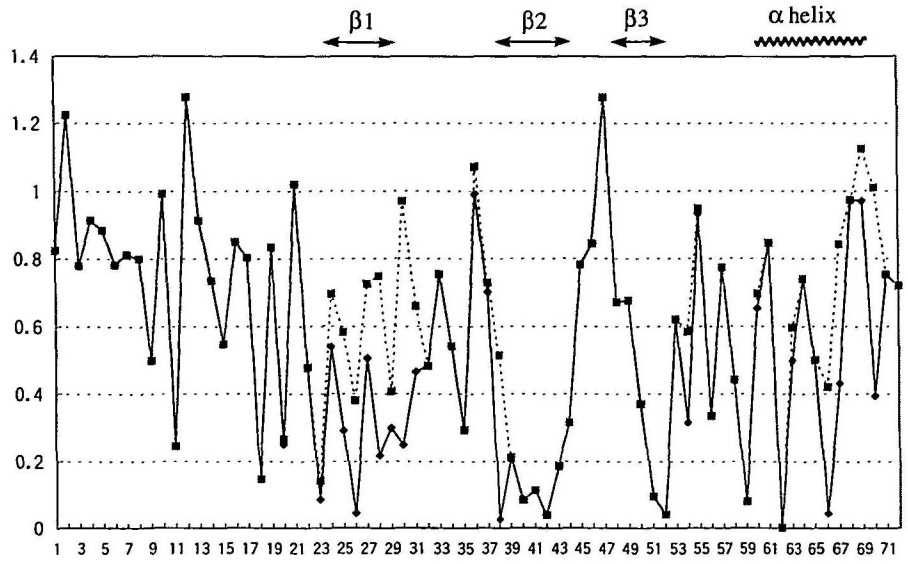

Fig. 7. **Plots of fractional solvent-accessible surface area for dimer and monomer CINC/Gro.** Calculations for the average structure were performed using a probe radius of 1.4 Å as a function of residual number. Fractional values were obtained by dividing by those of the extended conformation ($\phi = 180°$, $\psi = 0°$) of CINC/Gro.

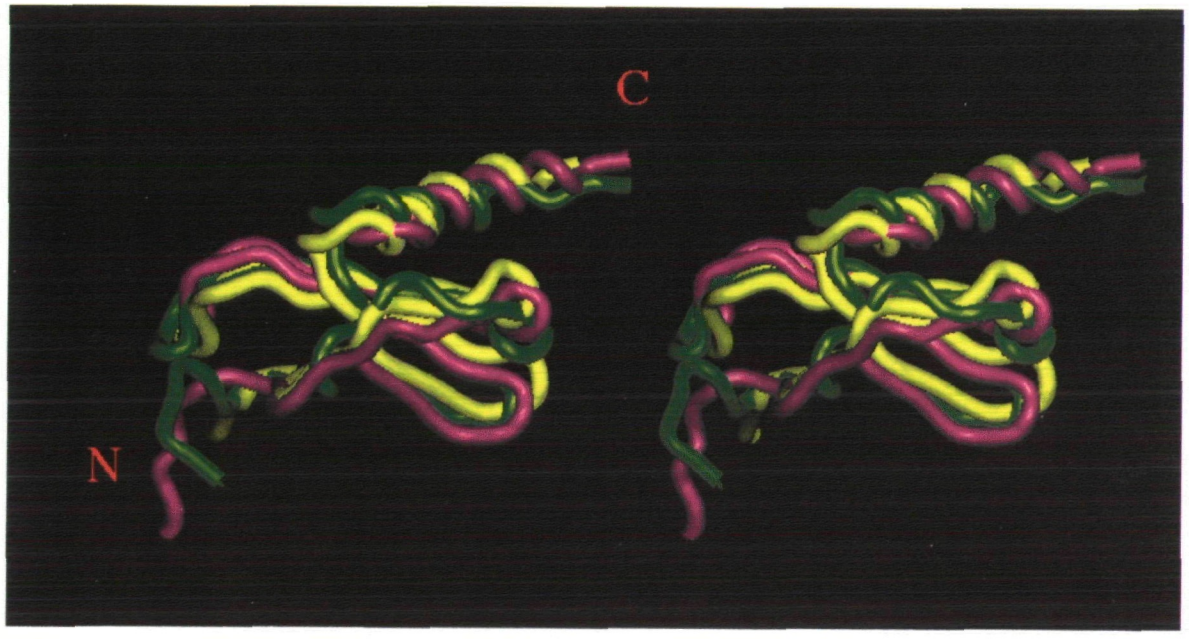

Fig. 8. **Comparison of the monomer structures of CINC/Gro and MGSA.** Best-fit superposition of the average structures of CINC/Gro (purple) and two human MGSA structures (green for 1MSG.pdb and yellow for 1mgs.pdb)was calculated based on the backbone atoms of residues 9-68. The average structure for 1mgs.pdb was calculated from 25 simulated annealing structures.

studies revealed that the monomer form is dominant at physiological concentrations in most CXC chemokines, including CINC/Gro (*35, 38, 39*). The monomeric form of IL-8 was directly shown to be the active entity (*40*). However, the comparison of interhelical distances among CXC chemokines in the dimeric states is still an effective means of evaluating the physicochemical properties of the individual chemokines, as well as the quality of the determined structure.

In human CXC chemokines, N-terminal ELR residues have been recognized to be essential for receptor binding. CINC/Gro also has an ELR motif, and deletion of the N-terminal 6 residues (from Val to Glu) of CINC/Gro reduced the chemotactic activity to one-tenth (*41*). Thus, the ELR motif is also responsible for binding to rat neutrophil receptor. The orientation of the ELR motif is not well defined in CINC/Gro, like other chemokines, though the presence of NOEs between Leu7 δCH_3 and C2H of His34 suggested that Leu7 sidechains do not protrude outward but are in contact with the protein core. The necessity of the scaffold of ELR for receptor binding is partly supported by the fact that N-terminal small peptides with an ELR sequence did not show chemotactic activity. The loop from 30 to 38 as the probable scaffold of ELR shows high r.m.s.d. values between CINC/Gro. This is not surprising, because significant conformational differences of the corresponding loop were also observed between NMR and X-ray structures of IL-8. This loop may be in multiple conformational

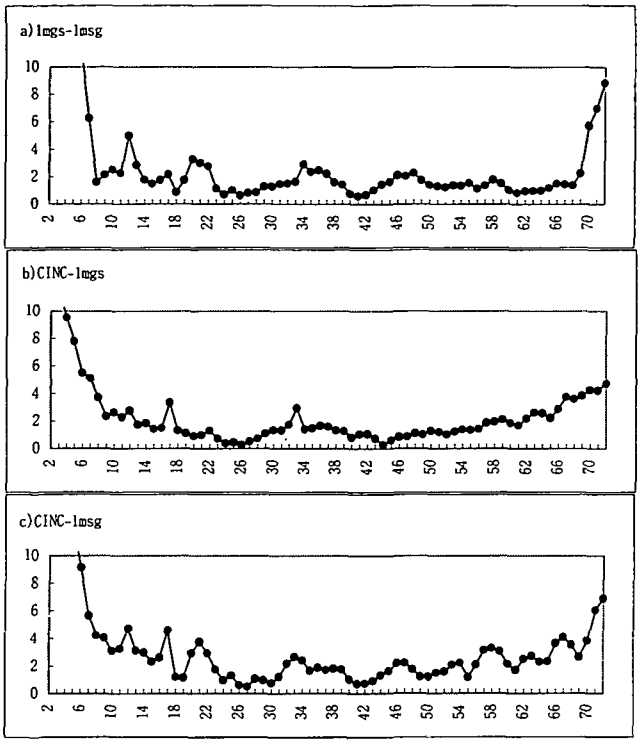

Fig. 9. **Plot of residue-based r.m.s. differences of backbone atoms between CINC/gro and human MGSA when superposition is optimized using residues 9 to 68.**

states. Since the change of His34 to Ala did not affect the activity in IL-8, His34 itself is not essential for the activity. In the loop region (Leu12-Lys21), which was assumed to be involved in the second binding region to the receptor, the sidechains of His19 and Lys21 are exposed to the solvent, as are the corresponding residues in IL-8. Based upon the fact that the N-terminal fragment peptide of CINC/Gro receptor affected the ^{1}H and ^{15}N chemical shifts of the residues from Val15 to His19 in HSQC experiments (data will be published elsewhere), these exposed basic residues are expected to be responsible for the interaction with the rather acidic N-terminal extracellular region of the CINC/Gro receptor. The his residue at this position is conserved in CXC chemokine in humans. The replacement of His19 of human MGSA by Ala reduced the chemotactic activity for neutrophils (7). Interestingly, in CINC 2-α and CINC 2-β, which are homologues of CINC/Gro (a rat counterpart of hMGSA), and have chemotactic activity for neutrophils, His at position 19 is replaced with Asp. It is not known whether CINC/Gro and CINC 2-α and CINC 2-β share the same receptor on neutrophil. The observation that the pK_a value of His19 is 5.8, which is significantly higher than that of MGSA (5.2), indicates that His 19 would be placed in a rather different environment. It is probable that such differences are associated with the selectivity of the chemokines to the specific receptors.

Supporting Information Available: ^{1}H, ^{13}C, and ^{15}N chemical shift assignments of CINC/Gro at 40°C, pH 5.3.

REFERENCES

1. Watanabe, K., Kinoshita, S., and Nakagawa, H. (1989) Purification and characterization of cytokine induced neutrophil chemoattractant produced by epithelioid cell line of normal rat kidney (NRK-52E cell). *Biochem. Biophys. Res. Commun.* **161**, 1093-1099
2. Watanabe, K., Konishi, K., Fujioka, M., Kinoshita, S., and Nakagawa, H. (1989) The neutrophil chemoattractant produced by rat kidney epithelioid cell line NRK-52E is a protein related to the KC/gro protein. *J. Biol. Chem.* **264**, 19559-19563
3. Nakagawa, H., Komorita, N., Shibata, F., Ikesue, A., Konishi, K., Fujioka, M., and Kato, H. (1994) Identification of cytokine induced neutrophil chemoattractant (CINC), rat Gro/CINC-2 alpha and CINC-2 beta, produced by granulation tissue in culture; purification, complete amino acid sequence and characterization. *Biochem. J.* **301**, 545-550
4. Baggiolini, M., Dewalds, B., and Moser, B. (1994) Interleukin 8 and related chemotactic cytokines: CXC and CC chemokines. *Adv. Immunol.* **55**, 97-179
5. Clore, B.M., Appella, E., Yamada, M., Matsushima, K., and Gronenborn, A.M. (1990) Three dimensional structure of interleukin-8 in solution. *Biochemistry* **29**, 1689-1696
6. Baldwin, E.T., Weber, I.T., Charles, R.St., Xuan, J.C., Appwlla, E., Yamada, M., Mitsushima, K., Edwards, B.F.P., Clore, G.M., Gronenborn, A.M., and Wlodawer, A. (1991) Crystal structure of interleukin 8: symbiosis of NMR and crystallography. *Proc. Natl. Acad. Sci. USA* **88**, 502-506
7. Fairbrother, W.J., Reilly, D., Colby, T.J., Hesselgesser, J., and Horuk, R. (1994) The solution structure of melanoma growth stimulating activity. *J. Mol. Biol.* **243**, 252-270
8. Kim, K.S., Clark-Lewis, I., and Sykes, B.D. (1994) Solution structure of GRO/melanoma growth stimulating activity determined by ^{1}H-NMR spectroscopy. *J. Biol. Chem.* **269**, 32909-32915
9. Lee, J., Horuk, R., Rice, G.C., Bennet, G.L., Camerato, T., and Wood, W.I. (1992) Characterization of two high affinity interleukin-8 receptors. *J. Biol. Chem.* **267**, 16283-16287
10. Cerretti, D.P., Kozlosky, C.J., Vanden Bos, T., Nelson, N., Gearing, D.P., and Beckman, M.P. (1993) Molecular characterization of receptors for human interleukin 8, gro/melanoma growth stimulating activity and neutrophil activating peptide-2. *Mol. Immunol.* **30**, 359-367
11. Gayle, R.B., Sleath, P.R., Srinivason, S., Birks, C.W., Weerawarna, K.S., Cerretti, D.P., Kozlosky, C.J., Nelson, N., Bos, T.V., and Beckman, M.T. (1993) Importance of the amino acid terminus of the interleukin 8 receptor in ligand interaction. *J. Biol. Chem.* **268**, 7283-7289
12. Ahuja, S.K., Lee, J.C., and Murphy, P.M. (1996) CXC chemokines bind to unique sets of selectivity determinants that can function independently and are broadly distributed on multiple domains of human interleukin 8 receptor B. *J. Biol. Chem.* **271**, 225-232
13. Clark-Lewis, I., Schumacher, C., Baggiolini, M., and Benhard, M. (1991) Structure-activity relationship of interleukin-8 determined using chemically synthesized analogs. *J. Biol. Chem.* **226**, 23128-23134
14. Hebert, C.A., Vitangcol, R.V., and Baker, J.B. (1991) Scanning mutagenesis of interleukin-8 identifies a cluster of residues required for receptor binding. *J. Biol. Chem.* **266**, 18989-18994
15. Clubb, R.T., Omichinski, J.G., Clore, G.M., and Gronenborn, A.M. (1994) Mapping the binding surface of interleukin-8 complexed with an N-terminal fragment of the type 1 human interleukin receptor. *FEBS Lett.* **338**, 93-97
16. Hanzawa, H., Haruyama, H., Watanabe, K., and Tsurufuji, S. (1994) The three dimensional structure of rat cytokine CINC/Gro in solution by homonuclear 3D NMR. *FEBS Lett.* **354**, 207-212
17. Lowman, H.B., Slagle, P.H., DeForge, L.E., Wirth, C.M., Gilece-Castro, B.L., Bourell, J.H., and Fairbrother, W.J. (1996) Exchanging interleukin-8 and melanoma growth-stimulating

activity receptor binding specificity. *J. Biol. Chem.* **271**, 14344-14352
18. Konishi, K., Takata, Y., Watababe, K., Date, Y., Yamamoto, M., Murase, M., Yoshida, H., Suzuki, T., Tsurufuji, S., and Fujioka, M. (1993) Recombinant expression of rat and human gro protein in *Escherichia coli*. *Cytokine* **5**, 506-511
19. Griesinger, C., Sorensen, O.W., and Ernst, R.R. (1987) Practical aspect of the E.COSY technique. Measurement of scalar spin-spin coupling constants in peptides. *J. Magn. Reson.* **75**, 474-492
20. Bax, Ad., Ikura, M., Kay, L.E., Torchia, D.A., and Tschudin, R. (1990) Comparison of different modes of two dimensional reverse-correlation NMR for the study of proteins. *J. Magn. Reson.* **86**, 304-318
21. Kay, L.E. and Bax, A. (1990) New methods for the measurements of NH-CαH coupling constants in ^{15}N-labeled proteins. *J. Magn. Reson.* **86**, 110-126
22. Grzesiek, S. and Bax, A. (1992) Improved 3D triple resonance NMR techniques applied to a 31 kDa protein. *J. Magn. Reson.* **96**, 432-440
23. Bax, A., Clore, G.M., and Gronenborn, A.M. (1990) H-H correlation via isotropic mixing of ^{13}C magnetization, a new three dimensional approach for assigning ^{1}H and ^{13}C spectra of ^{13}C enriched proteins. *J. Magn. Reson.* **88**, 425-431
24. Jeener, J., Meier, B.H., Bachmann, P., and Ernst, R.R. (1979) Investigation of exchange process by two dimensional NMR spectroscopy. *J. Chem. Phys.* **71**, 4546-4553
25. Ikura, M., Kay, L.E., Tschudin, R., and Bax, A. (1990) Three dimensional NOESY-HMQC spectroscopy of a ^{13}C-labeled protein. *J. Magn. Reson.* **86**, 204-209
26. Burgering, M.J.M., Boelens, R., Cafferey, M., Breg, J.N., and Kaptein, R. (1993) Observation of inter-subunit nuclear Overhauser effects in a dimeric protein. *FEBS Lett.* **330**, 105-109
27. Guntert, P., Brown, W., and Wüthrich, K. (1991) Efficient computation of the three-dimensional protein structures in solution from nuclear magnetic resonance data using the program DIANA and the supporting programs CALIBA, HABAS and GLOMSA. *J. Mol. Biol.* **217**, 507-530
28. Brunger, A.T. (1992) Xplor (version 3.1) Manual, Yale University Press, New Haven
29. Glasoe, P.K. and Long, F.A. (1960) Use of glass electrodes to measure acidities in deuterium oxide. *J. Phys. Chem.* **64**, 188-190
30. Chothia, C., Levitt, M., and Richardson, D. (1981) Helix to helix packing in protein. *J. Mol. Biol.* **145**, 215-250
31. Clore, G.M. and Gronenborn, A.M. (1991) Application of three and four dimensional heteronuclear NMR spectroscopy to protein structure determination. *Prog. NMR Spect.* **23**, 43-92
32. Senn, H., Werner, B., Messerle, B.A., Weber, C., Traber, R., and Wüthrich, K. (1989) Stereospecific assignment of the methyl ^{1}H NMR lines of valine and leucine in polypeptides by nonrandom ^{13}C labelling. *FEBS Lett.* **249**, 113-118
33. Guntert, P. and Wüthrich, K. (1991) Improved efficiency of protein structure calculations from NMR data using the program DIANA with redundant dihedral angle constraints. *J. Biomol. NMR* **1**, 447-456
34. Hyberts, S.G., Goldberg, M.S., Havel, T.F., and Wagner, G. (1992) The solution structure of eglin c based on measurements of many NOEs and coupling constants and its comparison with X-ray structures. *Protein Sci.* **1**, 736-751
35. Hanzawa, H., Haruyama, H., Konishi, K., Watanabe, K., and Tsurufuji, S. (1997) Subunit association and monomer structure of CINC/Gro revealed by ^{1}H-NMR. *J. Biochem.* **121**, 835-841
36. Charles, R.St., Walz, D.A., and Edwards, B.F.P. (1989) The three dimensional structure of bovine platelet factor 4 at 3.0 Å resolution. *J. Biol. Chem.* **264**, 2092-2099
37. Chothia, C. and Lesk, A.M. (1986) The relation between the divergence of sequence and structure in proteins. *EMBO J.* **5**, 823-826
38. Burrows, S.D., Doyle, M.L., Murphy, K.P., Franklin, S.G., White, J.R., Brooks, I., McNulty, D.E., Scott, M.O., Knutson, J.R., Porter, D., Young, P.R., and Hensley, P. (1994) Determination of the monomer-dimer equilibrium of Interleukin-8 reveals it is a monomer at physiological concentrations. *Biochemistry* **33**, 12741-12745
39. Schnitzel, W., Monschein, U., and Besemer, J. (1994) Monomer-dimer equilibria of interleukin-8 and neutrophil-activating peptide 2. Evidence for IL-8 binding as a dimer and oligomer to IL-8 receptor B. *J. Leuko. Biol.* **55**, 763-770
40. Rajarathnam, K., Sykes, B.D., Kay, C.M., Dewald, B., Geiser, T., Baggiolini, M., and Clark-Lewis, I. (1994) Neutrophil activation by monomeric interleukin-8. *Science* **264**, 90-92
41. Watanabe, K., Fujioka, M., Yokokawa, H., Konishi, K., Tsurufuji, S., and Nakagawa, H. (1992) Rat gro/melanoma growth-stimulating activity. Assessment of the structure responsible for chemotactic activity by use of its fragments prepared by proteolysis and chemical synthesis. *Cytokine* **4**, 12-19